Piebaldism and chromatophore development in reptiles are linked to the *tfec* gene

Highlights

- Captive-bred ball pythons show extensive Mendelian variation in pigmentation

- The recessive piebald phenotype is linked to a premature stop codon in *tfec*

- Mutated *tfec* inhibits development of iridophores in a lizard model

Authors

Alan Garcia-Elfring, Christina E. Sabin, Anna L. Iouchmanov, ...,
Andrew P. Hendry, Douglas B. Menke, Rowan D.H. Barrett

Correspondence

alan.garcia-elfring@mail.mcgill.ca
(A.G.-E.),
rowan.barrett@mcgill.ca (R.D.H.B.)

In brief

Garcia-Elfring et al. use population genetics, gene editing, and TEM imaging to show that a transcription factor is linked to white spotting in ball pythons and iridophore development in a lizard model.

Report

Piebaldism and chromatophore development in reptiles are linked to the *tfec* gene

Alan Garcia-Elfring,[1,6,*] Christina E. Sabin,[2,3] Anna L. Iouchmanov,[2] Heather L. Roffey,[4] Sukhada P. Samudra,[2] Aaron J. Alcala,[2] Rida S. Osman,[2] James D. Lauderdale,[3,5] Andrew P. Hendry,[1] Douglas B. Menke,[2] and Rowan D.H. Barrett[1,*]

[1]Department of Biology, Redpath Museum, McGill University, Montreal, QC H3A 0G4, Canada
[2]Department of Genetics, University of Georgia, Athens, GA 30602, USA
[3]Neuroscience Division of the Biomedical and Translational Sciences Institute, University of Georgia, Athens, GA 30602, USA
[4]Biology Department, Vanier College, Montreal, QC H4L 3X9, Canada
[5]Department of Cellular Biology, University of Georgia, Athens, GA 30602, USA
[6]Lead contact
*Correspondence: alan.garcia-elfring@mail.mcgill.ca (A.G.-E.), rowan.barrett@mcgill.ca (R.D.H.B.)
https://doi.org/10.1016/j.cub.2023.01.004

SUMMARY

Reptiles display great diversity in color and pattern, yet much of what we know about vertebrate coloration comes from classic model species such as the mouse and zebrafish.[1–4] Captive-bred ball pythons (*Python regius*) exhibit a remarkable degree of color and pattern variation. Despite the wide range of Mendelian color phenotypes available in the pet trade, ball pythons remain an overlooked species in pigmentation research. Here, we investigate the genetic basis of the recessive piebald phenotype, a pattern defect characterized by patches of unpigmented skin (leucoderma). We performed whole-genome sequencing and used a case-control approach to discover a nonsense mutation in the gene encoding the transcription factor *tfec*, implicating this gene in the leucodermic patches in ball pythons. We functionally validated *tfec* in a lizard model (*Anolis sagrei*) using the gene editing CRISPR/Cas9 system and TEM imaging of skin. Our findings show that reading frame mutations in *tfec* affect coloration and lead to a loss of iridophores in Anolis, indicating that *tfec* is required for chromatophore development. This study highlights the value of captive-bred ball pythons as a model species for accelerating discoveries on the genetic basis of vertebrate coloration.

RESULTS AND DISCUSSION

Color variation is one of the most visually striking forms of biodiversity and has a long history of study in evolutionary biology, as it is easily observed and is often important for survival.[1–3] Vertebrate color arises from pigments, structural coloration, and cell-cell interactions of three types of cells called chromatophores.[4,5] Mammals and birds have only a single type of chromatophore, the melanocyte, which produces the brown pigment melanin. In contrast, reptiles and other poikilothermic vertebrates have melanophores that produce melanin, but also xanthophores and iridophores. Xanthophores contain yellow to orange pteridine pigments[6,7] and are called leucophores when they show a white color and erythrophores if they contain red carotenoid pigments.[8,9] Iridophores do not contain pigment, but instead have guanine crystals that act as reflective platelets to produce structural coloration.[10] To date, the study of melanin-based pigmentation pathways has contributed the most to our understanding of pigmentation evolution and development in vertebrates.[11] Moreover, a limited number of classic model species like the mouse and zebrafish dominate the literature on pigmentation biology.[6,12–25] Importantly, however, the knowledge gained from these models might not translate to other vertebrate groups like reptiles, which remain less studied[26] (reviewed by Kuriyama et al.[27]). Ball pythons (*Python regius*), native to western sub-

Saharan Africa and a popular snake in the international pet trade, present an excellent opportunity to study the genetic basis of vertebrate coloration in an emerging reptile model.[28–30] Many Mendelian phenotypes ("base morphs"), representing rare, aberrant colorations,[31–33] have been discovered in nature and propagated in captivity. Ball python breeders have crossed these (inferred) single-gene color morphs to produce many more (inferred) multi-locus phenotypes ("designer morphs"; Figure 1). However, the actual genetic basis of these phenotypes remains largely unknown, with a few recent exceptions.[28,29]

We investigated the genetic basis for a classic color morph found in the pet trade and common across a wide range of vertebrate taxa, the piebald. This phenotype is characterized by leucodermic patches and has been described by commercial breeders as recessive.[34] Here, we analyze publicly available clutch data to investigate the mode of inheritance of the piebald phenotype in ball pythons and use whole-genome sequencing and population genomics to identify the genomic region likely containing the causal mutation. Through the annotation of genetic variants (SNPs and indels), we identified a candidate causal mutation in a gene coding for a transcription factor. We functionally validated this locus in a squamate model using CRISPR/Cas9 gene editing and confirmed an effect on chromatophore development by transmission electron microscopy (TEM) imaging.
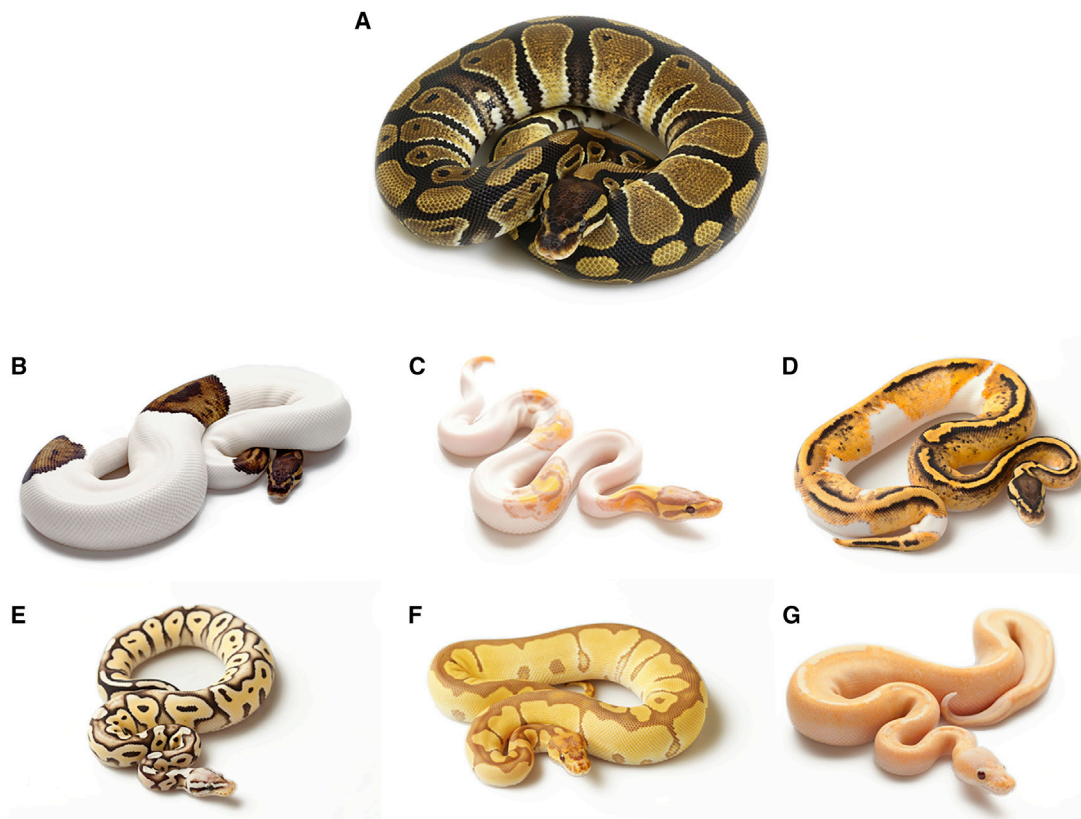
Figure 1. A small sample of the phenotypic variation found in captive-bred ball pythons (*Python regius*)
(A) Wild type, (B) piebald, (C) banana piebald, (D) pastel piebald, (E) pastel HRA enhancer, (F) ultramel clown, and (G) banana champagne. Photo credit: pethelpful. com (A) and *Designing Morphs* (B–G).

Mode of inheritance and delineation of genomic region of interest

To test whether the piebald phenotype segregates as a simple Mendelian factor, we compiled 10 years' worth of clutch data from a commercial breeder (*KINOVA*). Consistent with the knowledge among commercial breeders, the proportion of piebald hatchlings indicates the piebald phenotype is inherited as a recessive Mendelian factor (Figure 2A). We applied whole-genome pool-seq to two sets of individuals, one set with the piebald phenotype and another set inferred by commercial breeders through pedigree analysis to not have the piebald mutation or mutations. We obtained an average read coverage of 50.5 and 52.6 for the piebald and non-piebald pools, respectively. To map SNPs showing high differentiation between pools to genes, we aligned reads to the annotated Burmese python (*Python bivittatus*) draft genome (Pmo2.0), from which we obtained 3,095,304 SNPs after filtering. Across all SNPs, we found an average F_{ST} of 0.03456, indicating that population structure was successfully minimized. To delineate the genomic region of interest, we also mapped reads to a chromosome-length assembly. Using the draft assembly, we identified 129 fixed SNPs ($F_{ST} = 1.0$) and 369 SNPs with $F_{ST} > 0.9$ (Data S1A). Indeed, the chromosome-length assembly shows a single 8 Mb region of high differentiation on scaffold seven (7: 49526089–57612101), clearly delineating a genomic region of interest (Figure 2B).

Candidate genes and causal mutation

To obtain a list of candidate genes, we determined the gene annotations of variants with $F_{ST} > 0.90$ (Data S1B). We used $F_{ST} > 0.90$ (rather than $F_{ST} = 1$) to account for factors that might preclude finding a fixed causal mutation (e.g., sequencing error, misidentification of a sample, or minor sample contamination, as multiple snakes are often housed together by commercial breeders during breeding). We annotated SNPs for predicted loss of function to identify candidate causal mutations for the piebald phenotype. We found variants that mapped to the protein-coding sequences of 32 different genes. Most of the variants do not have a predicted effect on proteins, instead mapping to intronic and intergenic regions (344 "modifier" variants) and including one synonymous SNP (one "low"-impact mutation). The sole exception was a nonsense SNP (i.e., stop-gained mutation, "high" impact) with $F_{ST} = 0.96$ located within the fifth coding exon of the *tfec* gene (NW_006534020.1 160458). On the chromosome length assembly, exon five spans 7: 52856864–52856924. This variant consists of a c.493C>T (p.Arg165*) mutation, resulting in a premature opal termination codon. This mutation was validated by Sanger sequencing of *tfec* exon 5 and is expected to result in a truncated protein with functional domains missing (e.g., basic helix-loop-helix on exon 7). The coverage of the reference and alternative alleles is 1X and 47X in the piebald pool and 46X and 0X non-piebald
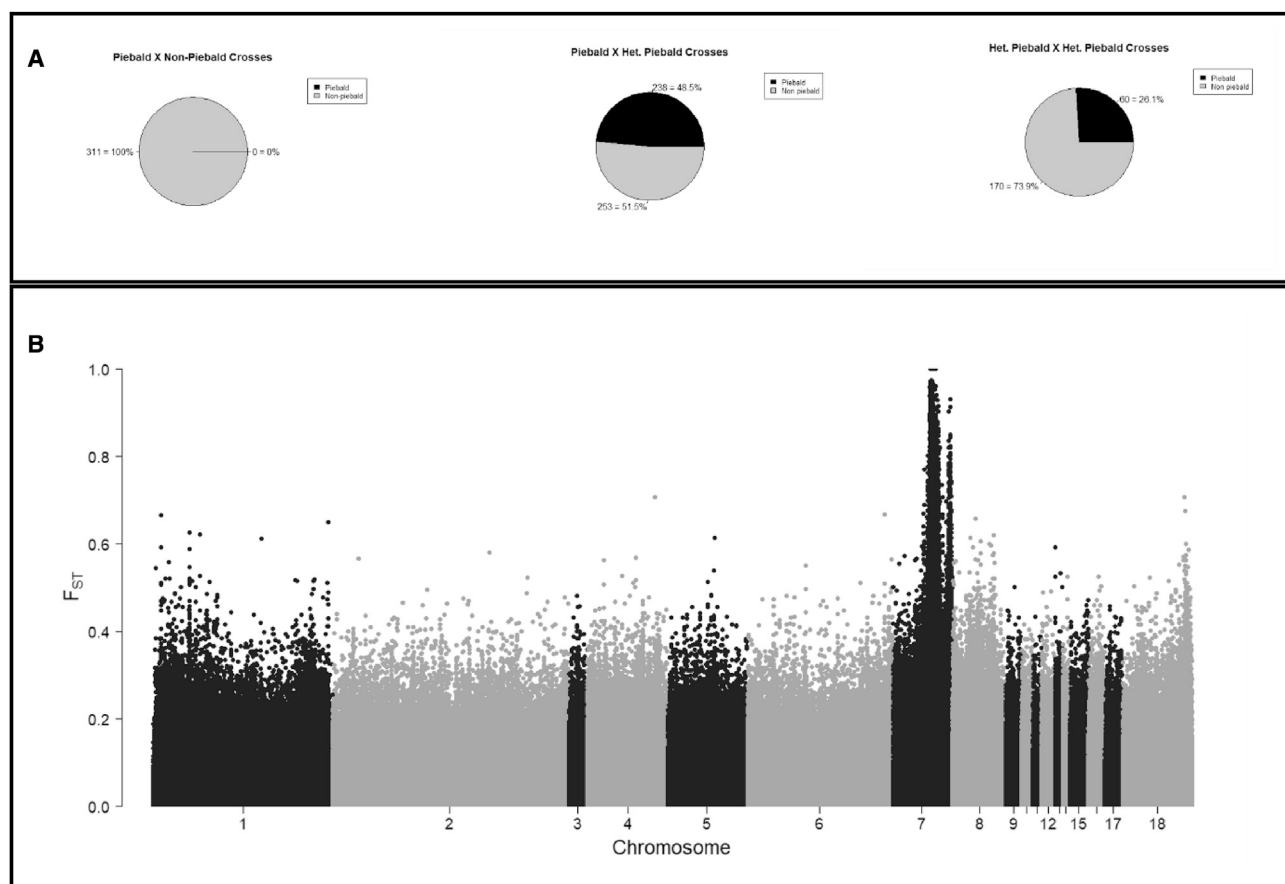
Figure 2. Inheritance patterns and genomic differentiation

(A) Clutch records (2008–2018) from a commercial breeder (*KINOVA*) indicate piebald has a recessive mode of inheritance.

(B) F_{ST} plot between piebald and non-piebald samples using a chromosome-length genome assembly. The F_{ST} peak on chromosome 7 delineates the region of interest containing the putative causal gene for the piebald phenotype.

pool, respectively. The single read for the reference allele sequenced in the piebald pool resulted in an F_{ST} below 1.00, potentially due to sample misidentification or minor contamination from co-housed animals. Among non-piebald samples, the reference allele is fixed.

Deletion of a splice acceptor site in snakes

To examine sequence conservation around the candidate variant, we generated a multispecies sequence alignment of the *tfec* coding exon five and flanking intronic sequence. This alignment revealed the presence of a 4 bp deletion in snakes at an intron-exon junction relative to other vertebrates (Figure S1). Our analyses of RNA-seq data from the brown anole lizard (*Anolis sagrei*) demonstrate that this snake-specific deletion removes one of two alternative splice acceptor sites (i.e., 3′ splice sites) that appear to be used in other squamates (Figure S2). We further note that certain other vertebrate species have single base pair changes that remove either splice site acceptor 1 (seen in some turtles) or splice site acceptor 2 (seen in some mammals, including humans). The use of splice acceptor 1 results in the inclusion of two additional codons relative to transcripts generated using splice acceptor 2. The functional differences, if any, between

tfec proteins generated by the two different splice acceptors are unknown. However, we infer that ball pythons likely use the second acceptor site, which is intact in ball pythons and other snakes. The stop codon mutation identified in piebald ball pythons occurs 6 bp from splice acceptor 2.

Targeted mutation of *tfec* in *Anolis* lizards

Protocols for genome editing in reptiles have been slow to develop because microinjection of single-cell embryos (zygotes) is difficult. To date, the brown anole lizard is the only squamate in which CRISPR/Cas9 has been successfully applied.[35] Therefore, to functionally validate *tfec* as a gene with a role in reptile coloration, we generated lizards with reading frame disrupting mutations in *tfec* coding exon 5, successfully producing four F0 mutant individuals. Mutant 1 carried one allele with a 56 bp deletion and a second allele with a 1 bp deletion, Mutant 2 carried a 190 bp inversion and a 295 bp deletion, Mutant 3 had a 4 bp deletion, and Mutant 4 had a 13 bp insertion. These lizards all exhibited altered pigmentation phenotypes (Figures S3A–S3D).

Relative to lizards with normal pigmentation (Figure 3A), the four F0 *tfec* mutants showed reduced coloration, particularly in the snout, arms, and legs (Figures 3B and S3A–S3D). In this
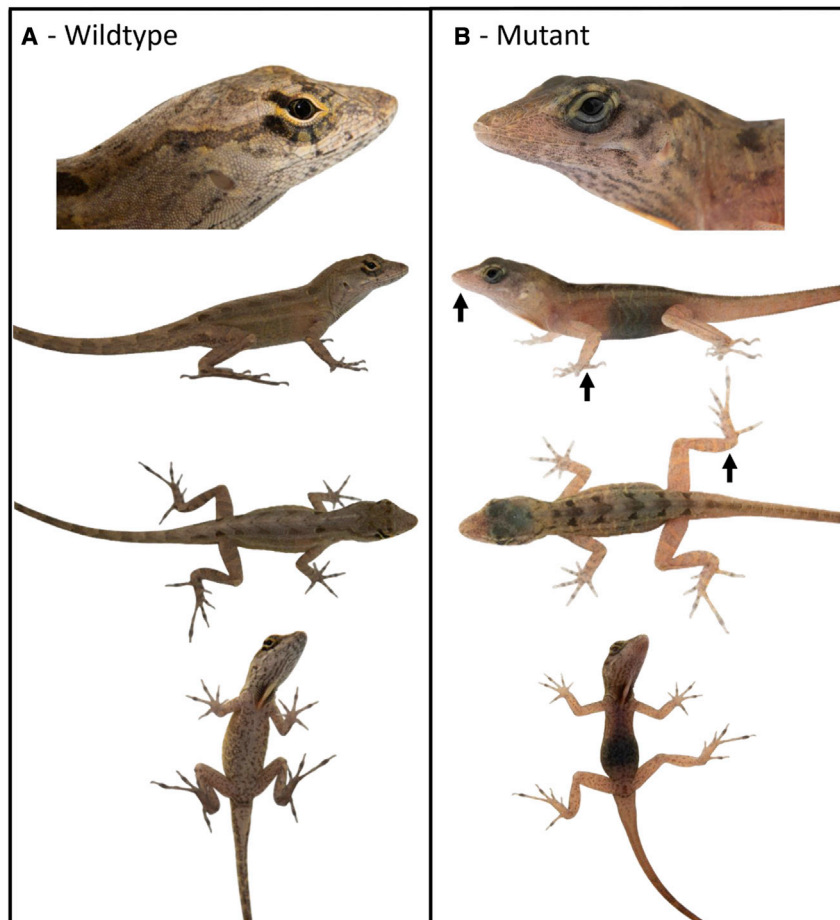
Figure 3. Phenotypic comparisons of *Anolis sagrei*
Wild type (A) and F0 *tfec* mutant (B). The mutant showed reduced body coloration, particularly in the snout, forelimbs, and hindlimbs (arrows).

(Figures 4 and S4). External examination of the eyes and skin revealed a loss of iridophores and presence of melanophores in *tfec*⁻/⁻ F1 hatchlings. The loss of the iridescent iridophores makes the eyes appear dark, much like the eyes of zebrafish that carry *tfec* mutations.[36] In contrast, *tyr*⁻/⁻ hatchlings retained iridophores but have an absence of melanophores. These changes in pigmentation were confirmed by TEM on skin samples. In wild-type skin, TEM readily detected melanosomes and guanine crystals, which are characteristic features of melanophores and iridophores, respectively. In contrast, melanosomes were absent *from tyr*⁻/⁻ skin and guanine crystals were absent from the skin of *tfec*⁻/⁻ hatchlings.

An MiTF/TFE transcription factor linked to reptile coloration

The *tfec* gene encodes a transcription factor from the MiT family of genes, which includes *mitf*, *tfe3*, *tfeb*, and *tfec*. These genes encode transcription factors that have basic helix-loop-helix and leucine zipper functional domains with important roles in lysosomal signaling, metabolism, and pigmentation.[37,38] *TFE3* and *TFEB* have pivotal roles in lysosomal acidification and autophagy,[39,40] while *MITF*, *TFE3*, and *TFEB* have all been linked to the development of cancer.[37,41,42] *MITF* is also considered a master regulator of melanocyte development[41] and was first discovered through its association with Waardenburg syndrome type II,[43] which is characterized by deafness, hypopigmentation, and microphthalmia.[44] Mutations to *mitf* in mammals have been shown to affect melanocyte differentiation, resulting in apoptosis[45] and leucodermic patches.[46,47] One of the few studies investigating snake pigmentation identified a mutation in *mitf* in leucistic Texas rat snakes[33]; this mutation, which results in an all-white phenotype, causes the loss of melanophores and xanthophores, but not iridophores.

Of the genes in the MiT family, the function of *tfec* is the least well understood,[48,49] but studies have shown that it is expressed, like *mitf*, in neural crest cells and retinal pigment epithelium of fish and mammals.[50–52] In mouse and zebrafish models, *mitf* and *tfec* are required for normal eye development.[49,50] Both *tfec* and *mitf* encode proteins with very similar helix-loop-helix domains,[51] and it has been proposed that these two transcription factors regulate gene expression together as heterodimers.[52] Kuiper et al.[53] studied the expression patterns of MiT genes in human tissues and showed that *tfec* and *mitf* have

respect, the mutant phenotype is like the reduced pigmentation observed in piebald ball pythons. However, in contrast to ball pythons, the anole mutants have black eyes and lack the leucodermic patches characteristic of the piebald phenotype. Lateral and ventral views also revealed that the skin of *tfec* mutants is translucent, allowing the internal organs and ribs to become more visible. We noted that Mutant 1 displayed small patches of skin on its head that were wild type in appearance, suggesting the possibility of mosaicism in this gene-edited animal (Figure S3A). Therefore, we generated F1 lizards to examine pigmentation patterns in the offspring of *tfec* mutants. Crossbreeding mutant F0s together demonstrated that, just as in ball pythons, *tfec* is not required for viability or fertility in brown anoles in captivity. All F1 progeny (n = 33) recapitulated the pigmentation phenotypes observed in the original F0 *tfec* mutants with no evidence of skin patches with wild-type pigmentation (Figure S3E).

To further understand the phenotype caused by our induced mutations, we examined the eyes and skin of *tfec* and *tyrosinase* (*tyr*) brown anole mutants and compared them to wild-type individuals. The gene *tyrosinase* was chosen as an additional control for these comparisons because of its role in melanin production. Through CRISPR/Cas9 editing, we targeted *tyr* and generated a line of *tyr* mutants that carry an 8 bp deletion in exon 2 of this gene. We dissected the eyes and skin from hatchlings homozygous for reading frame disrupting mutations in *tfec* or *tyr*
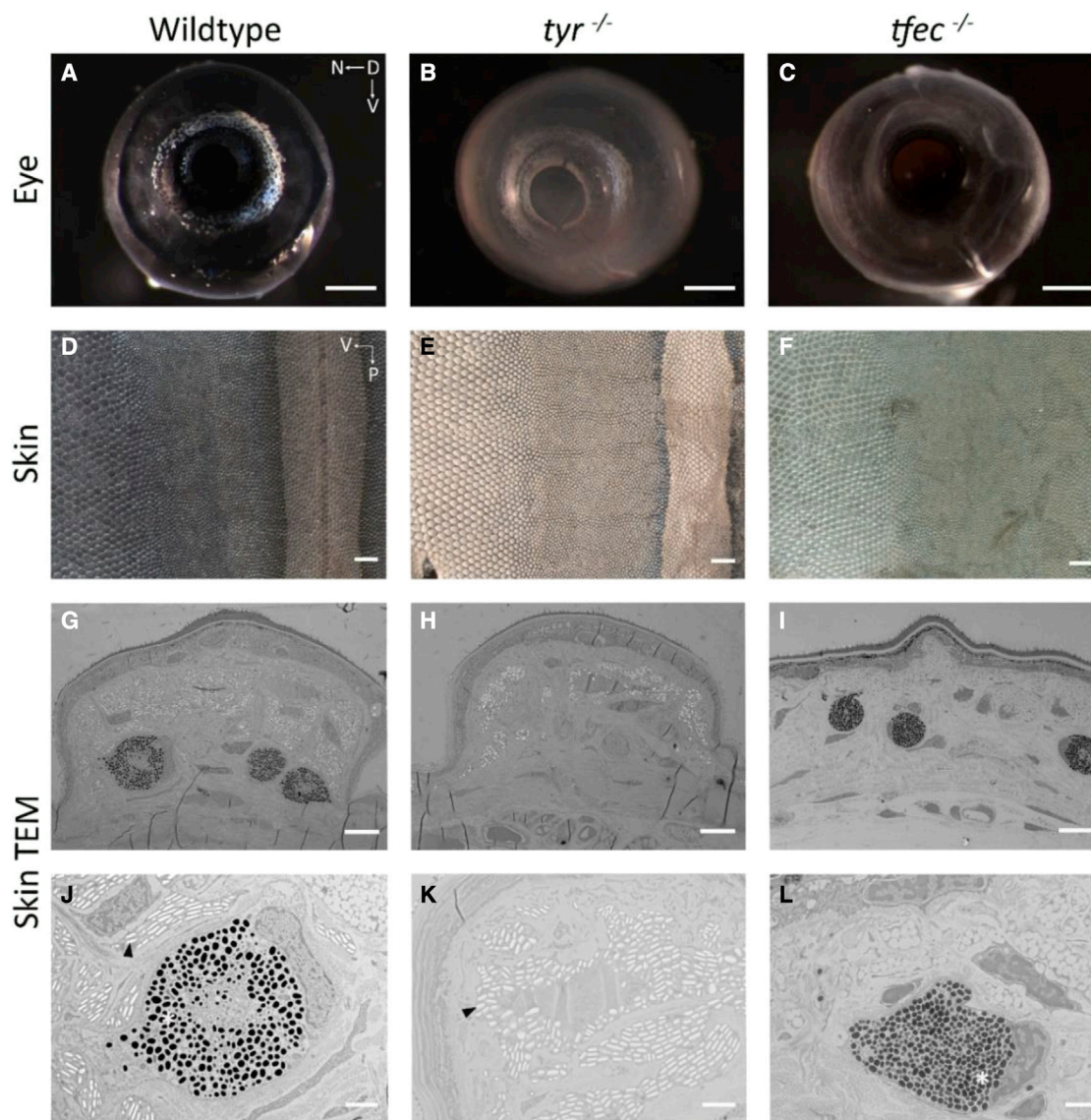
Figure 4. *tfec* is required for iridophore development in *Anolis sagrei*

Presented are eye and skin samples from wild type (A, D, G, and J) and mutants with reading frame mutations in *tyr* (B, E, H, and K) and *tfec* (C, F, I, and L).

(A–C) Anterior view of hatchling eyes.

(D–F) Dissected skin from the trunk of hatchlings. For these panels, anterior surface is up, and the posterior surface is down. Ventral surface is on the left side of the image and the dorsal surface is on the right. The dorsal stripe can be seen in (D) and (E) while (F) exhibits a lack of this back pattern.

(G–L) TEM images of individual dorsal scales (G–I) and higher-magnification images of melanophores and iridophores (J–L). Melanophores hold pigmented melanosomes while iridophore reflectiveness arises from guanine crystals. For $tyr^{-/-}$ note the absence of melanosomes and the presence of guanine crystals. For $tfec^{-/-}$ note the presence of melanosomes and the absence of guanine crystals. *tyr* samples are from F2 lizards; *tfec* samples are from F1 lizards. Asterisks show melanosomes while arrowheads point to guanine crystals.

Scale bars, (A–F) 500 μm, (G–I) 6 μm, (J–L) 2 μm.

multiple promoter regions and alternative splicing of functional domains, which may modulate target gene regulation.[48] Interestingly, they found that *tfec* displays the broadest variety of functionally distinct isoforms, with differential spatiotemporal tissue distribution (e.g., spleen, kidney, bone marrow, and small intestine). Although this study did not investigate the expression pattern in skin, the premature stop codon in the fifth exon of *tfec* found in piebald ball pythons is expected to result in a protein with missing basic helix-loop-helix and leucine zipper

functional domains, likely disrupting target gene regulation.[53] Our study adds *tfec* to the list of genes implicated in white spotting and pattern formation.[54,55]

tfec phenotypes in reptiles and other vertebrates

Identifying genes that affect color across a wide range of vertebrate species can lead to a deeper understanding of the mechanisms that underlie variation in color and pattern. Given the absence of iridophore and xanthophore cell types in mammals,

it is particularly important to expand functional genetic studies of pigmentation beyond mice to better understand the biology of these chromatophore cell types. For example, while we found that *tfec* affects reptile color, a mouse study showed that *tfec* mutants have normal coat pigmentation,[56] highlighting the need to study a wider range of taxa than traditional model organisms. Indeed, *tfec* was not included in a recent curated list of genes known to affect pigmentation.[16] However, more recent work on zebrafish has shown that *tfec* is required for iridophore cell fate specification.[36] Zebrafish *tfec* mutants also display delayed development of melanophores and xanthophores, but these chromatophores recover by day 4 post-fertilization. The *tfec*-associated phenotypes in reptiles and zebrafish contrast with reported *mitf* phenotypes in these species. In zebrafish, mutations to *mitf* result in a loss of melanophores, a reduction in xanthophores, and an increase in iridophore density.[57] In contrast, Texas rat snakes with a mutated *mitf* gene are leucistic (i.e., all white), lacking melanophores and xanthophores but showing no difference in iridophore density relative to the wild type.[33] Therefore, mutations in *tfec* and *mitf* produce distinct pigmentation phenotypes, with *mitf* playing a key role in melanophore development across vertebrates and *tfec* in iridophore development in fish and lizard models.

Our results support the conclusion that mutations to *tfec* in ball pythons cause piebaldism or white spotting, whereas in the brown anole they result in hypopigmentation and lack of iridophores. However, three main points remain unresolved. First is the question of what accounts for the species-specific differences in pigmentation phenotypes. It is known that ball pythons and lizards likely acquire their adult color pattern by different mechanisms.[5] Ball pythons have a fixed pattern specified in the embryo, prior to hatching and scale development, and as adults they do not show scale-by-scale coloration. In contrast, many lizards exhibit scale-by-scale coloration that is specified between the juvenile and adult stage. Thus, differences in the timing of gene expression of chromatophores may play a role in the species-specific differences in pigmentation phenotypes. Also unresolved is whether piebald ball pythons have iridophores in either pigmented or white skin. In the Texas rat snake, white coloration arises with iridophores present.[33] In the leopard gecko, skin from the ventral side is white but features a complete absence of all chromatophores.[58] Since *tfec* is required for iridophore development in both the brown anole and zebrafish, the white patches in piebald ball pythons may lack all chromatophores. However, TEM imaging will be needed to confirm the chromatophore content of piebald skin in ball pythons. A third point that requires further study is the role of the splice site deletion we detected in snakes and the function of different TFEC protein isoforms across reptile taxa. The splice site deletion itself does not cause piebaldism, since it is present in wild-type ball pythons and other snake species. However, two distinct splice acceptor sites are conserved across many squamate reptiles, and our data demonstrate that both acceptor sites are used in anoles. Whether the ability to produce different TFEC isoforms contributes to species-specific differences in *tfec* function remains to be tested.

In summary, the finding of a nonsense mutation associated with the piebald phenotype in ball pythons in combination with targeted mutation and TEM imaging in a brown anole model

shows *tfec* has an important role in reptile coloration. Mutations to *tfec* lead to hypopigmentation and a loss of iridophores in the skin and eyes of brown anoles. In snakes, *tfec* is likely to be required for the development of chromatophores migrating to body regions that correspond to leucodermic patches observed in piebald ball pythons. Our work highlights the advantages of using ball pythons as a model organism and working with non-academic communities like reptile breeders to accelerate discoveries in pigmentation research in an under-studied class of vertebrates.

STAR★METHODS

Detailed methods are provided in the online version of this paper and include the following:

- KEY RESOURCES TABLE
- RESOURCE AVAILABILITY
  - Lead contact
  - Materials availability
  - Data and code availability
- EXPERIMENTAL MODEL AND SUBJECT DETAILS
- METHOD DETAILS
  - Analysis of clutch data, sample collection, DNA extraction and sequencing
  - Bioinformatics
  - Functional validation of the putative piebald mutation in *Anolis sagrei*
  - Dissection of eyes and TEM imaging of skin
  - Gene nomenclature
- QUANTIFICATION AND STATISTICAL ANALYSIS

SUPPLEMENTAL INFORMATION

Supplemental information can be found online at https://doi.org/10.1016/j.cub.2023.01.004.

AUTHOR CONTRIBUTIONS

A.G.-E., A.P.H., and R.D.H.B. conceived the study and its design, with contributions from J.D.L. and D.B.M. H.L.R. collected and catalogued shed skin samples. A.G.-E. performed DNA extractions and bioinformatics to analyze whole-genome data. D.B.M. and J.D.L. carried out CRISPR/Cas9 project oversight. C.E.S. performed *in vitro* test of tfec CRISPR gRNA, preparation of *tfec* RNP, *tfec* surgeries and microinjection, breeding of *tfec*⁻/⁻ lizards, eye and skin dissections, stereomicroscope images, preparation of skin samples for TEM imaging, and working with the TEM microscopy technician. A.L.I. performed egg collection, egg care, screening hatchlings for phenotypes, documentation, and initial analysis of *tfec* phenotypes, genotyping, raising hatchlings, and breeding *tfec*⁻/⁻ lizards. S.P.S. performed *tfec* surgeries and microinjections. A.J.A. documented *tfec* phenotypes. R.S.O. was instrumental in the creation of the *tyrosinase* mutant line. J.D.L. contributed to the analysis of *tfec* phenotypes, project oversight, and project funding (NSF EDGE grant). D.B.M. performed *tfec* gene annotation, gRNA design, genotyping design, analysis of *tfec* phenotypes, project oversight, and project funding (NSF

REFERENCES

1. Caro, T. (2017). Wallace on coloration: contemporary perspective and unresolved insights. Trends Ecol. Evol. 32, 23–30. https://doi.org/10.1016/j.tree.2016.10.003.

2. Endler, J.A., and Mappes, J. (2017). The current and future state of animal coloration research. Philos. Trans. R. Soc. Lond. B Biol. Sci. 372, 20160352. https://doi.org/10.1098/rstb.2016.0352.

3. Davison, A., Jackson, H.J., Murphy, E.W., and Reader, T. (2019). Discrete or indiscrete? Redefining the colour polymorphism of the land snail Cepaea nemoralis. Heredity 123, 162–175.

4. Patterson, L.B., and Parichy, D.M. (2013). Interactions with iridophores and the tissue environment required for patterning melanophores and xanthophores during zebrafish adult pigment stripe formation. PLoS Genet. 9, e1003561.

5. Jahanbakhsh, E., and Milinkovitch, M.C. (2022). Modeling convergent scale-by-scale skin color patterning in multiple species of lizards. Curr. Biol. 32, 5069–5082.e13.

6. Ziegler, I. (2003). The pteridine pathway in zebrafish: regulation and specification during the determination of neural crest cell-fate. Pigment Cell Res. 16, 172–182. https://doi.org/10.1034/j.1600-0749.2003.00044.x.

7. Andrade, P., and Carneiro, M. (2021). Pterin-based pigmentation in animals. Biol. Lett. 17, 20210221. https://doi.org/10.1098/rsbl.2021.0221.

8. Fang, W., Huang, J., Li, S., and Lu, J. (2022). Identification of pigment genes (melanin, carotenoid and pteridine) associated with skin color variant in red tilapia using transcriptome analysis. Aquaculture 547, 737429.

9. Huang, D., Lewis, V.M., Foster, T.N., Toomey, M.B., Corbo, J.C., and Parichy, D.M. (2021). Development and genetics of red coloration in the zebrafish relative Danio albolineatus. eLife 10, e70253. https://doi.org/10.7554/eLife.70253.

10. Nicolaï, M.P.J., D'Alba, L., Goldenberg, J., Gansemans, Y., Van Nieuwerburgh, F., Clusella-Trullas, S., and Shawkey, M.D. (2021). Untangling the structural and molecular mechanisms underlying colour and rapid colour change in a lizard, Agama atra. Mol. Ecol. 30, 2262–2284.

11. McNamara, M.E., Rossi, V., Slater, T.S., Rogers, C.S., Ducrest, A.L., Dubey, S., and Roulin, A. (2021). Decoding the evolution of melanin in vertebrates. Trends Ecol. Evol. 36, 430–443. https://doi.org/10.1016/j.tree.2020.12.012.

12. Ishikawa, A., Sugiyama, M., Hondo, E., Kinoshita, K., and Yamagishi, Y. (2015). Development of a novel pink-eyed dilution mouse model showing progressive darkening of the eyes and coat hair with aging. Exp. Anim. 64, 207–220. https://doi.org/10.1538/expanim.14-0101.

13. Jackson, I.J. (1997). Homologous pigmentation mutations in human, mouse and other model organisms. Hum. Mol. Genet. 6, 1613–1624. https://doi.org/10.1093/hmg/6.10.1613.

14. Sturm, R.A. (2006). A golden age of human pigmentation genetics. Trends Genet. 22, 464–468. https://doi.org/10.1016/j.tig.2006.06.010.

15. Tsetskhladze, Z.R., Canfield, V.A., Ang, K.C., Wentzel, S.M., Reid, K.P., Berg, A.S., Johnson, S.L., Kawakami, K., and Cheng, K.C. (2012). Functional assessment of human coding mutations affecting skin pigmentation using zebrafish. PLoS One 7, e47398.

16. Baxter, L.L., Watkins-Chow, D.E., Pavan, W.J., and Loftus, S.K. (2019). A curated gene list for expanding the horizons of pigmentation biology. Pigment Cell Melanoma Res. 32, 348–358. https://doi.org/10.1111/pcmr.12743.

17. Feng, Y., McQuillan, M.A., and Tishkoff, S.A. (2021). Evolutionary genetics of skin pigmentation in African populations. Hum. Mol. Genet. 30, R88–R97. https://doi.org/10.1093/hmg/ddab007.

18. Ito, S., and Wakamatsu, K. (2011). Human hair melanins: what we have learned and have not learned from mouse coat color pigmentation. Pigment Cell Melanoma Res. 24, 63–74.

19. Sturm, R.A. (2009). Molecular genetics of human pigmentation diversity. Hum. Mol. Genet. 18, R9–R17.

20. Adhikari, K., Mendoza-Revilla, J., Sohail, A., Fuentes-Guajardo, M., Lampert, J., Chacón-Duque, J.C., Hurtado, M., Villegas, V., Granja, V., Acuña-Alonzo, V., et al. (2019). A GWAS in Latin Americans highlights the convergent evolution of lighter skin pigmentation in Eurasia. Nat. Commun. 10, 358.

21. Phelps, G.B., Hagen, H.R., Amsterdam, A., and Lees, J.A. (2022). MITF deficiency accelerates GNAQ-driven uveal melanoma. Proc. Natl. Acad. Sci. USA. 119. e2107006119.

22. Irion, U., and Nüsslein-Volhard, C. (2022). Developmental genetics with model organisms. Proc. Natl. Acad. Sci. USA. 119. e2122148119.

23. Seruggia, D., Josa, S., Fernández, A., and Montoliu, L. (2021). The structure and function of the mouse tyrosinase locus. Pigment Cell Melanoma Res. 34, 212–221.

24. Logan, D.W., Burn, S.F., and Jackson, I.J. (2006). Regulation of pigmentation in zebrafish melanophores. Pigment Cell Res. 19, 206–213.

25. Neuffer, S.J., and Cooper, C.D. (2022). Zebrafish syndromic albinism models as tools for understanding and treating pigment cell disease in humans. Cancers 14, 1752.

26. Kuriyama, T., and Hasegawa, M. (2017). Embryonic developmental process governing the conspicuousness of body stripes and blue tail coloration in the lizard Plestiodon latiscutatus. Evol. Dev. 19, 29–39.

27. Kuriyama, T., Murakami, A., Brandley, M., and Hasegawa, M. (2020). Blue, black, and stripes: evolution and development of color production and pattern formation in lizards and snakes. Front. Ecol. Evol. 8, 232.

28. Brown, A.R., Comai, K., Mannino, D., McCullough, H., Donekal, Y., Meyers, H.C., Graves, C.W., and Seidel, H.S.; BIO306W Consortium (2022). A community-science approach identifies genetic variants associated with three color morphs in ball pythons (Python regius). PLoS One 17, e0276376.

29. Dao, U.M., Lederer, I., Tabor, R.L., Shahid, B., Graves, C.W., and Seidel, H.S. (2022). Leucism and stripe formation in ball pythons (Python regius) are associated with variants affecting endothelin signaling. Preprint at bioRxiv. https://doi.org/10.1101/2022.10.09.511500.

30. Irizarry, K.J.L., and Bryden, R.L. (2016). In silico analysis of gene expression network components underlying pigmentation phenotypes in the Python identified evolutionarily conserved clusters of transcription factor binding sites. Adv. Bioinformatics 2016, 1286510.

31. Borteiro, C., Diesel Abegg, A., Hirouki Oda, F., Cardozo, D.E., Kolenc, F., Etchandy, I., Bisaiz, I., Prigioni, C., and Baldo, J.D. (2021). Aberrant colouration in wild snakes: case study in Neotropical taxa and a review of terminology. Salamandra 57, 124–138.

32. Iwanishi, S., Zaitsu, S., Shibata, H., and Nitasaka, E. (2018). An albino mutant of the Japanese rat snake (Elaphe climacophora) carries a nonsense mutation in the tyrosinase gene. Genes Genet. Syst. 93, 163–167.

33. Ullate-Agote, A., and Tzika, A.C. (2021). Characterization of the leucistic Texas rat snake Pantherophis obsoletus. Front. Ecol. Evol. *9*, 583136.

34. Barker, D.G., and Barker, T.M. (2006). Ball Pythons: The History, Natural History, Care and Breeding (VPI Library).

35. Rasys, A.M., Park, S., Ball, R.E., Alcala, A.J., Lauderdale, J.D., and Menke, D.B. (2019). CRISPR-Cas9 gene editing in lizards through microinjection of unfertilized oocytes. Cell Rep. *28*, 2288–2292.e3.

36. Petratou, K., Spencer, S.A., Kelsh, R.N., and Lister, J.A. (2021). The MITF paralog tfec is required in neural crest development for fate specification of the iridophore lineage from a multipotent pigment cell progenitor. PLoS One *16*, e0244794.

37. Slade, L., and Pulinilkunnil, T. (2017). The MiTF/TFE family of transcription factors: master regulators of organelle signaling, metabolism, and stress adaptation. Mol. Cancer Res. *15*, 1637–1643.

38. Hejna, M., Moon, W.M., Cheng, J., Kawakami, A., Fisher, D.E., and Song, J.S. (2019). Local genomic features predict the distinct and overlapping binding patterns of the bHLH-Zip family oncoproteins MITF and MYC-MAX. Pigment Cell Melanoma Res. *32*, 500–509.

39. Settembre, C., Di Malta, C., Polito, V.A., Garcia Arencibia, M., Vetrini, F., Erdin, S., Erdin, S.U., Huynh, T., Medina, D., Colella, P., et al. (2011). TFEB links autophagy to lysosomal biogenesis. Science *332*, 1429–1433.

40. Martina, J.A., and Puertollano, R. (2017). TFEB and TFE3: the art of multi-tasking under stress conditions. Transcription *8*, 48–54.

41. Levy, C., Khaled, M., and Fisher, D.E. (2006). MITF: master regulator of melanocyte development and melanoma oncogene. Trends Mol. Med. *12*, 406–414.

42. Goding, C.R., and Arnheiter, H. (2019). MITF—the first 25 years. Genes Dev. *33*, 983–1007.

43. Tassabehji, M., Newton, V.E., and Read, A.P. (1994). Waardenburg syndrome type 2 caused by mutations in the human microphthalmia (MITF) gene. Nat. Genet. *8*, 251–255.

44. Steingrímsson, E., Moore, K.J., Lamoreux, M.L., Ferré-D'Amaré, A.R., Burley, S.K., Zimring, D.C.S., Skow, L.C., Hodgkinson, C.A., Arnheiter, H., and Copeland, N.G. (1994). Molecular basis of mouse microphthalmia (mi) mutations helps explain their developmental and phenotypic consequences. Nat. Genet. *8*, 256–263.

45. Hu, S., Bai, S., Dai, Y., Yang, N., Li, J., Zhang, X., Wang, F., Zhao, B., Bao, G., Chen, Y., and Wu, X. (2021). Deubiquitination of MITF-M regulates melanocytes proliferation and apoptosis. Front. Mol. Biosci. *8*, 692724.

46. Hauswirth, R., Haase, B., Blatter, M., Brooks, S.A., Burger, D., Drögemüller, C., Gerber, V., Henke, D., Janda, J., Jude, R., et al. (2019). Correction: Mutations in MITF and PAX3 cause "SplashedWhite" and other white spotting phenotypes in horses. PLoS Genet. *15*, e1008321.

47. Baranowska Körberg, I., Sundström, E., Meadows, J.R.S., Rosengren Pielberg, G., Gustafson, U., Hedhammar, Å., Karlsson, E.K., Seddon, J., Söderberg, A., Vilà, C., et al. (2014). A simple repeat polymorphism in the MITF-M promoter is a key regulator of white spotting in dogs. PLoS One *9*, e104363.

48. Lister, J.A., Lane, B.M., Nguyen, A., and Lunney, K. (2011). Embryonic expression of zebrafish MiT family genes tfe3b, tfeb, and tfec. Dev. Dyn. *240*, 2529–2538.

49. Agostini, F., Agostinis, R., Medina, D.L., Bisaglia, M., Greggio, E., and Plotegher, N. (2022). The regulation of MiTF/TFE transcription factors across model organisms: from brain physiology to implication for neurodegeneration. Mol. Neurobiol. *59*, 5000–5023.

50. George, A., Zand, D.J., Hufnagel, R.B., Sharma, R., Sergeev, Y.V., Legare, J.M., Rice, G.M., Scott Schwoerer, J.A., Rius, M., Tetri, L., et al. (2016). Biallelic mutations in MITF cause coloboma, osteopetrosis, microphthalmia, macrocephaly, albinism, and deafness. Am. J. Hum. Genet. *99*, 1388–1394.

51. Rowan, S., Chen, C.-M.A., Young, T.L., Fisher, D.E., and Cepko, C.L. (2004). Transdifferentiation of the retina into pigmented cells in ocular retardation mice defines a new function of the homeodomain gene Chx10. Development *131*, 5139–5152.

52. Bharti, K., Gasper, M., Ou, J., Brucato, M., Clore-Gronenborn, K., Pickel, J., and Arnheiter, H. (2012). A regulatory loop involving PAX6, MITF, and WNT signaling controls retinal pigment epithelium development. PLoS Genet. *8*, e1002757.

53. Kuiper, R.P., Schepens, M., Thijssen, J., Schoenmakers, E.F.P.M., and van Kessel, A.G. (2004). Regulation of the MiTF/TFE bHLH-LZ transcription factors through restricted spatial expression and alternative splicing of functional domains. Nucleic Acids Res. *32*, 2315–2322.

54. Ahi, E.P., and Sefc, K.M. (2017). A gene expression study of dorso-ventrally restricted pigment pattern in adult fins of Neolamprologus meeli, an African cichlid species. PeerJ *5*, e2843.

55. Baxter, L.L., Hou, L., Loftus, S.K., and Pavan, W.J. (2004). Spotlight on spotted mice: a review of white spotting mouse mutants and associated human pigmentation disorders. Pigment Cell Res. *17*, 215–224.

56. Steingrímsson, E., Tessarollo, L., Pathak, B., Hou, L., Arnheiter, H., Copeland, N.G., and Jenkins, N.A. (2002). Mitf and Tfe3, two members of the Mitf-Tfe family of bHLH-Zip transcription factors, have important but functionally redundant roles in osteoclast development. Proc. Natl. Acad. Sci. USA *99*, 4477–4482.

57. Lister, J.A., Robertson, C.P., Lepage, T., Johnson, S.L., and Raible, D.W. (1999). Nacre encodes a zebrafish microphthalmia-related protein that regulates neural-crest-derived pigment cell fate. Development *126*, 3757–3767.

58. Szydłowski, P., Madej, J.P., and Mazurkiewicz-Kania, M. (2016). Ultrastructure and distribution of chromatophores in the skin of the leopard gecko (E ublepharis macularius). Acta Zool. *97*, 370–375.

59. Sedlazeck, F.J., Rescheneder, P., and Von Haeseler, A. (2013). NextGenMap: fast and accurate read mapping in highly polymorphic genomes. Bioinformatics *29*, 2790–2791.

60. Li, H., Handsaker, B., Wysoker, A., Fennell, T., Ruan, J., Homer, N., Marth, G., Abecasis, G., and Durbin, R.; 1000 Genome Project Data Processing Subgroup (2009). The sequence alignment/map format and SAMtools. Bioinformatics *25*, 2078–2079.

61. Kofler, R., Orozco-terWengel, P., De Maio, N., Pandey, R.V., Nolte, V., Futschik, A., Kosiol, C., and Schlötterer, C. (2011). PoPoolation: a toolbox for population genetic analysis of next generation sequencing data from pooled individuals. PLoS One *6*, e15925.

62. Kofler, R., Pandey, R.V., and Schlötterer, C. (2011). PoPoolation2: identifying differentiation between populations using sequencing of pooled DNA samples (Pool-Seq). Bioinformatics *27*, 3435–3436.

63. Cingolani, P., Platts, A., Wang, L.L., Coon, M., Nguyen, T., Wang, L., Land, S.J., Lu, X., and Ruden, D.M. (2012). A program for annotating and predicting the effects of single nucleotide polymorphisms, SnpEff: SNPs in the genome of Drosophila melanogaster strain w1118; iso-2; iso-3. Fly *6*, 80–92.

64. Concordet, J.-P., and Haeussler, M. (2018). CRISPOR: intuitive guide selection for CRISPR/Cas9 genome editing experiments and screens. Nucleic Acids Res. *46*, W242–W245.

65. Castoe, T.A., de Koning, A.P.J., Hall, K.T., Card, D.C., Schield, D.R., Fujita, M.K., Ruggiero, R.P., Degner, J.F., Daza, J.M., Gu, W., et al. (2013). The Burmese python genome reveals the molecular basis for extreme adaptation in snakes. Proc. Natl. Acad. Sci. USA *110*, 20645–20650.

66. Wysoker, A., Tibbetts, K., and Fennell, T. (2013). Picard tools version 1.90. https://sourceforge.net/projects/picard/files/picard-tools/1.90/.

67. Dudchenko, O., Batra, S.S., Omer, A.D., Nyquist, S.K., Hoeger, M., Durand, N.C., Shamim, M.S., Machol, I., Lander, E.S., Aiden, A.P., and Aiden, E.L. (2017). De novo assembly of the Aedes aegypti genome using Hi-C yields chromosome-length scaffolds. Science *356*, 92–95.

68. Dudchenko, O., Shamim, M.S., Batra, S.S., Durand, N.C., Musial, N.T., Mostofa, R., Pham, M., St Hilaire, B.G., Yao, W., and Stamenova, E. (2018). The Juicebox Assembly Tools module facilitates de novo assembly of mammalian genomes with chromosome-length scaffolds for under $1000. Preprint at bioRxiv. https://doi.org/10.1101/254797.

69. Chong, J.X., Buckingham, K.J., Jhangiani, S.N., Boehm, C., Sobreira, N., Smith, J.D., Harrell, T.M., McMillin, M.J., Wiszniewski, W., Gambin, T., et al. (2015). The genetic basis of Mendelian phenotypes: discoveries, challenges, and opportunities. Am. J. Hum. Genet. *97*, 199–215.

70. Geneva, A.J., Park, S., Bock, D., de Mello, P., Sarigol, F., Tollis, M., Donihue, C., Reynolds, R.G., Feiner, N., Rasys, A., et al. (2021). Chromosome-scale genome assembly of the brown anole (Anolis sagrei), a model species for evolution and ecology. Preprint at bioRxiv. https://doi.org/10.1101/2021.09.28.462146.

71. Mehravar, M., Shirazi, A., Nazari, M., and Banan, M. (2019). Mosaicism in CRISPR/Cas9-mediated genome editing. Dev. Biol. *445*, 156–162.

72. Lewis, A.C., Rankin, K.J., Pask, A.J., and Stuart-Fox, D. (2017). Stress-induced changes in color expression mediated by iridophores in a polymorphic lizard. Ecol. Evol. *7*, 8262–8272.

73. Reynolds, E.S. (1963). The use of lead citrate at high pH as an electron-opaque stain in electron microscopy. J. Cell Biol. *17*, 208–212.

STAR★METHODS

KEY RESOURCES TABLE

REAGENT or RESOURCE	SOURCE	IDENTIFIER
Biological samples		
Ball python shed skin from 47 piebald 52 non-piebald individuals	Commercial breeders (Mutation Creation, T. Exotics, The Ball Room, Desinging Morphs)	N/A
Chemicals, peptides, and recombinant proteins		
Proteinase K	Thermo Fisher Scientific	cat#EO0491
Phenol:Chloroform:Isoamyl Alcohol 25:24:1, Saturated with 10mM Tris, pH 8.0, 1mM EDTA	Thermo Fisher Scientific	cat#15593049
Picogreen	Thermo Fisher Scientific	cat#P11495
Deposited data		
FASTQ	This paper	SRA: PRJNA924959
Experimental models: Organisms/strains		
Ball python (*Python regius*)	Captive-bred	N/A
Oligonucleotides		
Primers for Sanger sequencing (genotyping) in ball pythons: Tfec exon 5 Forward: 5'-AACTCAGAGCACTCCATGACC-3'; Reverse: 5'-CAGGTGTGCCCCTTTCATAA-3'	This paper	N/A
tfec Cas9 RNP: Targets sites 5'-AGAAACAGATACACGAGCAA-3' and 5'-AGATACACGAGCAATGGCAA-3'	This paper	N/A
tyr Cas9 RNP: Target site 5'-ATGATAAAGGGAGGACACCT-3'	This paper	N/A
Primers for Sager sequencing in brown anole: Tfec-F3: 5'-AAGGGCACATGGCTTGGAAG-3' and Tfec-R3: 5'-CAGTGGGTCTATACTAAACCTGA-3'; Tfec-468-F: 5'-CCATGTACCATTTATCAATGCTATGC-3' and Tfec-1121-R: 5'-CATCGAATTGTTGCCAATCTGTG-3'	This paper	N/A
Software and algorithms		
NextGenMap	Sedlazeck et al.[59]	https://cibiv.github.io/NextGenMap/
Samtools	Li et al.[60]	http://www.htslib.org/download/
Popoolation	Kofler et al.[61]	https://sourceforge.net/projects/popoolation/
Popoolation2	Kofler et al.[62]	https://sourceforge.net/projects/popoolation2/
SnpEff	Cingolani et al.[63]	http://pcingola.github.io/SnpEff/
CRISPOR	Concordant and Haeussler[64]	http://crispor.tefor.net/
R	R Foundation	https://www.r-project.org/

RESOURCE AVAILABILITY

Lead contact
Further information should be directed to lead contact Alan Garcia-Elfring (alan.garcia-elfring@mail.mcgill.ca).

Materials availability
This study did not generate new unique reagents.

Data and code availability

Raw sequence data are available at SRA: PRJNA924959

EXPERIMENTAL MODEL AND SUBJECT DETAILS

Shed skin from ball pythons (*Python regius*) was provided by commercial breeders. Short read sequencing data was acquired from pooled DNA of snakes with the piebald phenotype (n = 47) and snakes inferred by commercial breeders through pedigree analysis to not have the piebald mutation or mutations (n = 52). Subject details reported in this paper can be found in the STAR Methods and Data S1C and S1D.

METHOD DETAILS

Analysis of clutch data, sample collection, DNA extraction and sequencing

To test whether the piebald phenotype segregates as a simple Mendelian factor, we compiled 10 years' worth of clutch data available online data from a commercial breeder (*KINOVA*). We included data from piebald relevant crosses (https://kinovareptiles.com/incubator/?clutch_id=piebald): piebald vs. inferred non piebald, piebald vs. inferred heterozygotes, and crosses between inferred heterozygotes. We obtained ball python samples (shed skin) by appealing to commercial breeders from Canada (Mutation Creation, T. Dot Exotics, The Ball Room Canada, Designing Morphs). We used a case-control approach, using shed skin samples from 47 piebald individuals (inferred to be homozygous for the piebald variant; Data S1C) and 52 non-piebald individuals (inferred to be homozygous wild-type from pedigrees; Data S1D). Although individuals from both sets of samples contained additional mutations (i.e., other base morphs), the only consistent difference between the two pools was the piebald versus non-piebald phenotype difference. We attempted to maximize the number of individuals that came from different families to minimize the effects of population structure, although there were some exceptions (Data S1D). From each sample, we used approximately 0.1 g of shed skin, cut to small pieces using scissors, for DNA extraction. We extracted DNA following a standard phenol-chloroform procedure, with the modification of a 24-hour proteinase-K incubation time at 37 °C. Piebald and non-piebald samples were prepared on different working days to avoid contamination. We quantified all samples using a Picogreen ds DNA assay (Thermo Fisher Scientific, Waltham, USA) on an Infinite 200 Nanoquant (Tecan Group Ltd. Männedorf, Switzerland). After DNA extraction, we mixed DNA of individuals (according to phenotype) in equimolar amounts to obtain a single pool for each phenotype, 'piebald' and 'non-piebald.' Because extracted DNA from shed skin was degraded, we used PCR-based whole-genome libraries for both pools. We sequenced 150 bp pair-end reads on two lanes of Illumina HiSeqX. Library preparation and DNA sequencing were done at the McGill University and Genome Quebec Innovation Center in Montreal, Canada. The locus of interest (*tfec* exon 5) was validated with PCR and Sanger sequencing.

Bioinformatics

We processed raw reads by filtering for read quality and length with the program *Popoolation*.[61] We kept reads with a minimum quality of 20 (–quality-threshold 20) and a length of 50 bp (–min-length 50). We then aligned processed reads to the Burmese python (*Python bivittatus*) draft assembly Pmo2.0[65] using the program *NextGenMap*.[59] *NextGenMap* was designed for aligning reads to highly polymorphic genomes or genomes of closely related species. We used *SAMtools*[60] to convert SAM files to BAM format and remove reads with mapping quality below 20 (samtools view -q 20). PCR duplicates were removed with the program *MarkDuplicates* of *Picard Tools*.[66] We used the *Popoolation2*[62] protocol to produce a sync file, which contains read counts for all nucleotides sequenced in the genome and used this for subsequent downstream analyses (e.g., F_{ST} scan). In a separate analysis, we applied the same protocol as above but instead aligned reads to the chromosome-length Burmese python reference genome, Python_molurus_bivittatus-5.0.2_HiC.assembly.[67,68]

We applied a genome-wide F_{ST} scan to search for SNPs showing high differentiation between the two pools. For this procedure, we used the *fst-sliding.pl* script of *Popoolation2* (–min-count 10, –min-coverage 20, –max-coverage 500, –min-covered-fraction 0, –window-size 1, –step-size 1, –pool-size 47:52, –suppress-noninformative). We then identified SNPs with high F_{ST} estimates (F_{ST} = 0.9-1.0) and mapped them to genes. We used a custom script to map SNPs with high differentiation to genes in the gene annotation file using the scaffold name and SNP position. Because the draft assembly of the Burmese python is highly fragmented,[65] we also applied the same F_{ST} scan on data aligned to the chromosome-length genome assembly[67,68] – thus obtaining better delineation of the genomic region of interest. However, this latter assembly is not annotated with genetic features, hence necessitating the use of both assemblies.

Mendelian phenotypes arise predominantly due to mutations to the protein-coding sequences of genes.[69] We thus annotated variants (SNPs and indels) with the software *snpEff*[63] to aid in identifying the putative causal mutation for the piebald phenotype within protein-coding genes. *SnpEff* was designed for annotating and predicting loss or reduced function effects of variants on gene protein-products, such as amino acid changes. This program provides an assessment of the impact of a variant, including 'HIGH' (e.g., stop codon), 'MODERATE' (e.g., non-synonymous change), 'LOW' (e.g., synonymous change), or 'MODIFIER' (change in an intergenic area).

Functional validation of the putative piebald mutation in *Anolis sagrei*

Gene editing was performed on wild-caught brown anole females under the approval and oversight of the University of Georgia Institutional Animal Care and Use Committee (A2019 07-016-Y3-A3). All experiments followed the National Research Council's Guide for

the Care and Use of Laboratory Animals. CRISPR/Cas9 genome editing was carried out as previously reported[35] with the following modifications: For analgesia, rimadyl (4 μg/g) was substituted for meloxicam, and the Cas9 RNP concentration was increased to 10 μM Cas9 RNP was produced by mixing SpCas9 2NLS with sgRNA (Synthego Corp, Menlo Park, CA) in 10 mM Tris-HCl, pH 7.4. In addition, Cas9 RNP was injected into a maximum of three follicles per ovary, prioritizing the largest follicles. The size of follicles injected ranged from 1mm to 10mm in diameter, and included both previtellogenic and large, yolky follicles. Potential guide sites were obtained using *tfec* coding exon 5 from the *A. sagrei* AnoSag2.1 assembly,[70] and targets were chosen using CRISPOR 4.4,[64] selecting targets with Fusi-Scores of 50% or greater. Before performing oocyte injections, we tested the ability of the Cas9 RNP to digest a PCR product than spans the target site. An equal mixture of two sgRNA was used to create *tfec* Cas9 RNP: Targets sites 5' AGAAACAGATACACGAGCAA 3' and 5' AGATACACGAGCAATGGCAA 3'. A total of 44 follicles in 12 adult females were injected to generate four *tfec* mutants. For the production of the *tyr* mutant line, a single sgRNA directed against *tyr* exon 2 was used to create *tyr* Cas9 RNP: Target site 5'ATGATAAAGGGAGGACACCT.

Eggs from CRISPR injected females were collected and incubated at 29°C. Upon hatching, lizard tail clips were collected, and genomic DNA prepared. Hatchlings were screened for mutations in *tfec* coding exon 5 by performing Sanger Sequencing on two different PCR amplicons: 466bp *tfec* amplicon (Tfec-F3: 5'-AAGGGCACATGGCTTGGAAG-3' and Tfec-R3: 5'-CAGTGGGTCTA TACTAAACCTGA-3'); 1595bp *tfec* amplicon (Tfec-468-F: 5'-CCATGTACCATTTATCAATGCTATGC-3' and Tfec-1121-R: 5'-CATC GAATTGTTGCCAATCTGTG-3'). Sanger sequencing revealed mutations in two male (*Mutant 1* and *Mutant 3*) and two female (*Mutant 2* and *Mutant 4*) hatchlings. *Mutant 1* and *mutant 2* carried mutant alleles with large size differences that allowed us to gel purify two distinct PCR bands of different sizes from each lizard. We sequenced these gel purified bands to obtain clean chromatograms and verify the sequence of the mutant alleles. All mutations shifted the *tfec* reading frame. No evidence of wild-type alleles was detected in the mutants. Only wild-type alleles were detected in lizards with normal pigmentation. To test for germline transmission, *Mutant 1* was crossed with *Mutant 2* and *Mutant 4*. Mutations in *tyr* were identified as previously described.[35] We note that in many vertebrates, F0 genome edited individuals are highly mosaic.[71] Injecting Cas9 RNP into immature lizard oocytes that are not fertilized for days to weeks allows for an extended period for Cas9 RNP to enter the nucleus and cut the target site on the maternal allele (and upon fertilization) the paternal allele. We speculate that may account for the low mosaicism that we observed in the F0 mutants.

Dissection of eyes and TEM imaging of skin

F0 *tfec* mutants were crossed to generate F1 *tfec-/-* progeny that we used for more detailed analyses of eyes and skin. An F0 *tyr* mutant male heterozygous for an 8bp deletion in *tyr* exon 2 was crossed to produce heterozygous F1 lizards; F1 *tyr-/+* lizards were then intercrossed to produce F2 *tyr-/-* lizards. Wild-type, *tyr-/-*, and *tfec -/-* hatchlings were euthanized, and their eyes and skin from the trunk were collected immediately. The freshly dissected tissue was imaged using a ZEISS Discovery V12 SteREO microscope, AxioCam (MRc5), and Axio Vision 4.8.2 (release 06-2010). Electron microscopy was performed following the protocol of Lewis et al. (2017)[72] with modification. Samples were fixed in 2.5% glutaraldehyde in phosphate-buffered saline (PBS) overnight at room temperature. Fixed tissue samples were rinsed three times in PBS for 10 min each, before being dehydrated in increasing concentrations of ethanol consisting of 25%, 50%, 70%, 80%, 90%, 100%, and 100% anhydrous ethanol for 60 min each. Following dehydration, the cells were infiltrated with increasing concentrations of LR White resin in ethanol consisting of 25%, 50%, 75%, and 100% resin for 6 hr each step. After a second change of 100% resin, the samples were embedded in fresh resin in gelatin capsules. The gelatin capsules were capped to exclude air and the resin polymerized in an oven at 60°C for 24 h. The embedded tissues in resin blocks were sectioned with a diamond knife on a Leica Ultracut S microtome and ultrathin sections (60-70 nm) were collected onto formvar-coated 100 mesh hexagonal copper grids. The sections on grids were sequentially stained with 2% aqueous uranyl acetate for 30 min and Reynolds Lead Citrate for 8 min[73] and viewed in JEOL JEM-1011 transmission electron microscope at 80-100 kV. Images were captured with an AMT XR80M Wide-Angle Multi-Discipline Mid-Mount CCD digital camera, at a resolution of 3296 x 2460 pixels.

Gene nomenclature

Throughout this article, we follow gene nomenclature established in humans and zebrafish. In humans, gene names are capitalized (e.g., *TFEC* and *MITF*), whereas when referring to genes in other model organisms (e.g., zebrafish, mouse, and reptiles) the gene names are presented in lowercase letters (e.g., *tfec* and *mitf*) for simplicity.

QUANTIFICATION AND STATISTICAL ANALYSIS

F_{ST} was estimated using the *fst-sliding.pl* script of *Popoolation2*.[62] F_{ST} estimates were visualized using R version 4.2.1. All additional information can be found in Method details.